Heterostructure and Compositional Depth Profile of Low-temperature Processed Lead Titanate Based Ferroelectric Thin Films Prepared by PhotoChemical Solution Deposition

*I. Bretos[1], R. Jiménez[1], E. Rodriguez-Castellón[2], J. García-López[3] and M.L. Calzada[1]

[1] *Instituto de Ciencia de Materiales de Madrid, C.S.I.C., Cantoblanco 28049 Madrid, Spain*

[2] *Departamento de Química Inorgánica, Facultad de Ciencias, Universidad de Málaga, 29071 Málaga, Spain*

[3] *Centro Nacional de Aceleradores (C.N.A.), Parque Tecnológico Cartuja 93, 41092 Sevilla, Spain*

Keywords: X-ray Photoelectron Spectroscopy, Rutherford Backscattering Spectroscopy, ultraviolet sol-gel photoannealing, ferroelectric, thin films

Abstract. The heterostructure and compositional depth profile of low-temperature processed $(Pb_{0.76}Ca_{0.24})TiO_3$ (PCT24) ferroelectric thin films have been studied in the present work. The films were prepared by ultraviolet (UV) sol-gel photoannealing (also called PhotoChemical Solution Deposition, PCSD) onto platinised silicon substrates and crystallised at 450 ºC in air and oxygen atmospheres. Despite using such a low temperature, analysis carried out by X-ray Photoelectron Spectroscopy (XPS) revealed the total lack of organic rests within the bulk film. Complementary information about the heterostructure of the films was also obtained by Rutherford Backscattering Spectroscopy (RBS). Both analytical techniques detected the presence of a lead gradient in the films, together with small fluctuations on the concentration of this element along the bulk film. The RBS study also showed that the films of this work develop a Pt_xPb interface between the ferroelectric layer and the Pt bottom electrode. The thickness of this interlayer is much lower than that of the interface formed in PCT24 films prepared at higher temperatures (650 ºC) without UV-irradiation (conventional CSD). On the other hand, the low processing temperature here used minimises the lead loss by volatilisation, as deduced from the RBS simulated spectra of the films. Thus, the lead excess incorporated in the precursor solution remains in the films after the crystallisation treatment. This result would suppose a significant advance towards the environmentally low-impact processing of lead-containing ferroelectric films with applications in electrical and electronic components (e.g. piezoelectric devices).

1. Introduction

Since the strong development of the microelectronic industry in the 80s, ferroelectric materials in thin film form are being exploited in an extensive deal of commercial devices making use of their unique piezo-, pyro- and ferroelectric properties.[1] The integration of the ferroelectric active layer into the silicon circuit[2] ("integrated ferroelectric") is the crucial fact that has allowed the fabrication of novel electronic micro/nano-devices such as piezoelectric actuators, infrared sensors and ferroelectric memories[3] (non-volatile and dynamic random access memories). There exist several multioxide ferroelectric compositions which have fairly proved their competitiveness in such applications, e.g. $Pb(Zr,Ti)O_3$ (PZT), $SrBi_2Ta_2O_9$ (SBT), $Bi_4Ti_3O_{12}$ (BiT) and $(Ba,Sr)TiO_3$ (BST).[1] However, all of them have a common handicap that prevents their compatibility with the silicon technology, that is, the high processing temperature (over 600 ºC) at which the film is normally treated, which may produce serious damage to the Si-based semiconductor substrate.[4] Besides, the use of these temperatures also favours the interdiffusion among the different layers of the device, thus promoting the formation of detrimental interfaces that affect negatively the electrical response of the material.[5] One of the major failure mechanisms hindering ferroelectric switching-devices commercialization (the polarisation loss with repeated bipolar switching cycles, known as fatigue), is directly related to processes occurring in the ferroelectric layer-bottom metal electrode interface.[6] Therefore, the reduction of the processing temperature of ferroelectric thin films is one of the key-topics of the ferroelectric community nowadays.

Ferroelectric $(Pb_{0.76}Ca_{0.24})TiO_3$ (PCT24) thin films have been widely studied in the light of pyroelectric detectors and MicroElectroMechanical System (MEMS) due to their high values of pyroelectric coefficient[7] ($\gamma = 42 \times 10^{-9}$ C/cm^{2}ºC) and piezoelectric d_{33} coefficient[8] (d_{33} = 70 pm/V), which make them highly competitive to other solid solution systems employed in these applications. Among the different physical and chemical techniques used for the preparation of ferroelectric thin films, Chemical Solution Deposition (CSD) methods (mainly sol-gel and Metalloorganic Decomposition) offer the particular advantage of tailoring the solution chemistry to aim the challenge of the low-temperature fabrication of these materials.[9-15] In 2004, some authors of this work made use of the ultraviolet (UV) sol-gel photoannealing technique in ferroelectric multioxide compositions to prepare single-phase perovskite PCT24 films

at 450 ºC with optimum dielectric and ferroelectric response.[16] A description of the major applications of the UV-light on thin films, out of the scope of this work, can be found in reference (17). More recently (2007), the same authors[18] have revealed the superior electrical properties of the PCT24 films when they are UV-irradiated under oxygen local atmosphere, due to the lower density of defects and oxygen vacancies in the bulk film (ozonolysis effect)[19]. Continuing in the same research line, we want now to deep insight the effect of the low-temperature processing on the heterostructure and compositional features of the resulting oxide films, which highly determines their dielectric and ferroelectric response and thus, their use in functional electronic devices.

The majority of works reporting on the fabrication of ferroelectric thin films at low temperatures are mainly focused on securing phase-pure crystalline structure and suitable ferroelectric activity at such low temperatures, since amorphous rests and secondary phases (e.g. pyrochlore) that spoil the ferroelectric response are stabilised at these temperatures. To the best knowledge of the authors, few publications are found in the literature that address the particular effect of the low-temperature processing on the heterostructure of the crystalline films obtained. Probably, the most significant result regarding this topic is the identification in lead titanate based films of a metastable intermetallic phase located at the interface between the ferroelectric layer and the bottom metal electrode,[20] principally observed in PZT films deposited onto Pt coated silicon substrates during the early states of annealing. The composition of this transient phase, which varies depending on the annealing conditions, is generally referred to Pt_xPb, and its influence on the preferred orientation of the low-temperature processed films has been thoroughly discussed.[21-23] The thickness of this interlayer determined by Transmission Electron Microscopy (TEM) and Rutherford Backscattering Spectroscopy (RBS) in amorphous PZT films (400 ºC/5 min) is, as example, near 10 % of total film thickness.[24] Until the present time, however, the study of this intermetallic layer has been restricted to films belonging to the PZT system. It would be interesting to test the formation of this particular interface in other ferroelectric thin films based on the lead titanate perovskite. On the other hand, we expect that the low processing temperature here used (450 ºC) might lead to a decrease on the lead volatilisation of the films of this work. This would suppose a significant advance towards the environmentally low-impact processing of lead titanate based ferroelectric films making use of relative clean technologies. Compositional studies carried out by electron probe x-ray microanalysis

on UV-irradiated PZT films revealed a decrease on the lead and oxygen concentrations at temperatures above 500 ºC.[25] Also, High Oxygen-Pressure Processing (HOPP) of low–temperature (400 ºC) prepared PZT films is supposed to decrease the lead and oxygen losses and therefore to reduce the density of oxygen vacancies,[26] although these phenomena were not supported by any compositional analysis. In general, Electron Probe Microanalysis (EPMA) techniques are based on the identification of the elements of which the specimen (e.g. thin film) is composed. Stoichiometry of the sample is then calculated from the ratio among the different elements concentrations. The experimental configuration of the surface analytical techniques here used (XPS and RBS) allows determining not only the average nominal composition of the film in an accurate manner, but also the compositional depth profile of the sample. This provides the advantage of denoting the presence of chemically different interfacial layers and concentration fluctuations[22] along the film.

Summarising, we present a systematic study of the particular heterostructure and compositional depth profile of the PCT24 ferroelectric films obtained by ultraviolet sol-gel photoannealing at 450 ºC, using air and oxygen atmospheres. The XPS and RBS analyses conducted on the films provide specific information about the film-electrode interface developed at this low temperature and the influence of the annealing conditions (temperature, local atmosphere) on the lead volatilisation and composition of the films.

2. Experimental Section

2.1. Sample Preparation

The fabrication of the PCT24 films of this work was already described elsewhere.[18] It can be summarised as follows: a precursor solution leading to $(Pb_{0.76}Ca_{0.24})TiO_3$ nominal composition was prepared by a diol-based sol-gel process. The solution was initially synthesised with a 10 mol% excess of Pb^{2+} and deposited onto $Pt/TiO_2/SiO_2/(100)Si$ substrates by spin-coating. The as-deposited films were dried on a hot-plate at 150 ºC for 5 min. The gel films thus obtained were subjected to ultraviolet irradiation at 250 ºC for 4 min and subsequently crystallised at 450 ºC for 1 h by means of an UV-assisted rapid thermal processor (UV-RTP),[16,18] using air or oxygen atmospheres. In order to obtain samples of a desired thickness, the films comprised a

total of four layers. Each layer was individually deposited, dried, UV-irradiated and crystallised. The films thus prepared will be here denoted as PCT24-air or PCT24-ox, depending on the atmosphere used in the thermal treatment (air or oxygen, respectively).

2.2. Sample Characterisation

X-Ray Diffraction (XRD) analysis was used to determine the presence of crystalline phases in the films processed at 450 ºC. Conventional Bragg-Brentano measurements were carried out in a Siemens D500 powder diffractometer using CuK_α radiation and a scan step of 0.05º (2θ) per 3 s.

The heterostructure and depth profiling of the films was analysed by X-ray Photoelectron Spectroscopy (XPS). A standard x-ray source, 15 kV, 300 W, Mg Kα (1253.6 eV) was used for these measurements. The pressure in the analysis chamber was ~10^{-7} Pa. Survey and multiregion spectra were recorded of Ca 2p, Pb 4f, O 1s, Ti 2p, Pt 4f, Si 2p and C 1s photoelectron peaks. Binding energies were referenced to Ca $2p_{3/2}$ at 347.0 eV. Depth profiling was carried out using a 4 keV Ar^+ bombardment at a current density of ~1.5 μA/cm^2. A crater of about 1mm diameter was studied. The in-depth scale of 4.5 nm/min was assumed to be equivalent to the sputter rate of Ta_2O_5 under the same sputter conditions.

Rutherford Backscattering Spectroscopy (RBS) was also performed to further study the compositional profile and heterostructural features of the films. Experimental equipment involved a 3 MV Tandem-type Van de Graaff accelerator with a 3 MeV $^4He^{2+}$ (low weight) or 7 MeV $^{14}N^+$ (high weight) beam. The backscattered ions were collected with a silicon surface barrier detector set at 165º. The RBS experimental data were analysed using the SIMNRA[27] simulation code. Error in the calculation of the composition was 10 %. Bulk densities of the PCT24 layer of 7.15 g/cm^3 and of the Pt bottom electrode of 21.40 g/cm^3 were considered for the calculation of the thickness. These values are the theoretical densities of these compounds, thus considering in the calculation that the different constituent layers of the heterostructure have a bulk density of 100 %.

2.3. PCT24 film prepared by conventional CSD at 650 ºC without UV-irradiation

A PCT24 film prepared by conventional Chemical Solution Deposition (CSD) and treated by Rapid Thermal Processing (RTP) in air at high temperature (650 ºC),

without using UV-irradiation, was selected for the sake of comparison with the films of this work. The precursor solution thereby used contained a 10 mol% excess of Pb^{2+} and it was synthesised by the same diol-based sol-gel route followed to prepare the low-temperature processed films here shown. Details concerning the fabrication, heterostructure and electrical response of this film (with nomenclature PCT24-air*) can be found in references (28,29).

3. Results

Figure 1 shows the XRD patterns of the PCT24-air and PCT24-ox films processed at 450 ºC by PCSD. Peaks corresponding to a single-phase perovskite (Pv) crystalline structure can be observed in the diffractograms without any secondary phase or rest of amorphous detected. The dash line depicted at $2\theta = 38.5^{o}$ is attributed to the (111) reflection of an fcc Pt_xPb intermetallic phase.[11,20-24] Small peaks can be inferred from the XRD patterns of the films close to this 2θ value, although the strong <111> orientation of the Pt bottom electrode prevents a more precise identification. Attending to the possible presence of texture in the films, a clear <100> preferred orientation is observed for the PCT24-air film, whereas this orientation results much lower in the PCT24-ox film. Information about the <111> direction cannot be here obtained due to the overlapping between the 111 perovskite peak of the film and the 111 Pt peak of the bottom electrode.

The analysis obtained by XPS during depth profiling of the films is shown in Figure 2. The atomic concentration of the constituent elements of the PCT24-air (Fig. 2a) and PCT24-ox (Fig. 2b) films versus sputter time is depicted in this figure. Preferential loss of lead occurs during first minutes of Ar^+ sputtering due to the high volatility of this element.[30] However, after several minutes of Ar^+ bombardment, a steady-state situation is reached in the sample which is representative of the bulk film. Further depth profiling reveals the heterostructure of the substrate; the Pt electrode, the TiO_2 layer and the (100)Si substrate. Note how the signals of the respective Ti 2p and O 1s core levels increase after the maximum of Pt 4f level appears, which is ascribed to the TiO_2 buffer layer present in the substrate ($Pt/TiO_2/SiO_2/(100)Si$). Assuming a sputter rate of 4.5 nm/min (Ta_2O_5), thicknesses of ~195 and ~205 nm are calculated by XPS for the PCT24-air and PCT24-ox films, respectively. Insets of this figure show the

individual signal of the Pb 4f core level obtained during depth profiling of the respective films. The atomic concentration of this element seems to slightly increase as the analysis is focused towards the inner layers of the ferroelectric film, before reaching the substrate (a straight line is depicted in the graphs to show this tendency). Small fluctuations on the lead content along the film can also be inferred from these graphs, although the preferential sputtering of this element at the beginning of the analysis prevents its realistic quantification.

Figure 3 shows the binding energy spectra of the C 1s and O 1s core levels measured during depth profiling of the PCT24-air film. Identical results were obtained for the PCT24-ox film, which have been omitted from this figure. At the beginning of the analysis, the experimental signal of the C 1s level shows peak maxima at ~284.7 and ~287.8 eV (Fig. 3a). These binding energies correspond to adventitious carbon and carbon from carbonate groups, respectively.[31] The photoemission peaks at these values of the C 1s core level disappear from the spectra of the film after 1 min of sputtering cleaning with Ar^+. In the case of the O 1s spectrum (Fig. 3b), the signal obtained during the first minutes of Ar^+ sputtering reveals two different peaks with maxima at ~529.9 and ~532.5 eV. The former peak is attributed to oxygen atoms of CO_3^{2-} (carbonate) groups and those of the PbO oxide[32] that is preferentially sputtered at the beginning of the Ar^+ bombardment. After 1 min of sputtering cleaning, only the later peak (~532.5 eV) corresponding to oxygen atoms of the $(Pb_{0.76}Ca_{0.24})TiO_3$ perovskite is observed in the O1s spectra.

The RBS experimental and simulated spectra of the PCT24-air film measured with a 3 MeV $^4He^{2+}$ beam are shown in Figure 4. The use of light α-particles ($^4He^{2+}$ ions) allows detecting elements of the sample with a low backscattering energy. Thus, the complete heterostructure of the film is shown in this figure, where the bulk film, the Pt bottom electrode and the TiO_2 buffer layer are observed. A lead gradient with a concentration increasing from the top to the bottom is deduced from the simulated spectrum of the PCT24-air film. For the further discussion of these results, inset of Fig. 4 shows a plan-view micrograph of the film obtained by Scanning Electron Microscopy (SEM). Regions with different contrast can be observed in the micrograph which correspond to areas with variations in height (up to around 15 nm) ascribed to the presence of roughness in the sample surface.[18]

To get deeper information about the films heterostructure, RBS measurements were also performed with a 7 MeV $^{14}N^{+}$ beam and both experimental and simulated spectra obtained are shown in Figure 5 (a and b for the PCT24-air and PCT24-ox film, respectively). From these data, the heterostructure deduced for both films is depicted and included in the figure. Note that the use of a heavier energetic beam ($^{14}N^{+}$ incident ions) provides measurements with a high resolution and makes possible to infer the four constituent layers of each film from the experimental data obtained. Thus, the spectra show a compositional discontinuity from one layer to another, where a drop in the amount of lead is simulated (indicated by arrow heads). This result would support those previously observed in Fig. 2, where the XPS analysis carried out in the films denoted compositional fluctuations on the lead content along the bulk film in both samples (see insets of Fig. 2). The lead gradient detected by the RBS measurements of Fig. 4, with a concentration increasing towards the inner layers, is also observed here. From the RBS simulated spectra of Fig. 5, an average elemental composition of 0.84 Pb + 0.24 Ca + 1.00 Ti + 3.08 O♠ (±10 % error) is calculated for both PCT24-air and PCT24-ox films. The presence of an interfacial layer between the ferroelectric film and the Pt bottom electrode is also detected by the RBS analysis. This interface is around 4 % of total film thickness and has a composition close to that of a Pt_xPb intermetallic compound. From the RBS data, thicknesses of ~272 and ~290 nm are calculated for the PCT24 films processed in air or oxygen, respectively. The calculated thickness of the Pt bottom electrode is also indicated in the figure.

A summary of the most important heterostructural features deduced by XPS and RBS for the PCT24 films of this work is shown in Table 1. Dielectric and ferroelectric characterisation of these films was also performed and results are recently reported in reference (18). The most significant electrical parameters thus obtained appear collected in this table. Data corresponding to the PCT24-air* film (conventional CSD at high temperature without UV-irradiation) are also included.[28,29]

4. Discussion

The use of two different but complementary analytical techniques for the study of thin-film materials, such as X-ray Photoelectron Spectroscopy (XPS) and Rutherford

♠ The atomic concentration of oxygen has been determined from the atomic concentrations calculated by RBS in the metal cations (Pb, Ca, Ti)

Backscattering Spectroscopy (RBS), have allowed us to gain insight the heterostructural features of the low-temperature processed ferroelectric thin films of this work.

In the XPS analysis, the preferential loss of lead observed during the first minutes of Ar^+ sputtering prevents the possibility of obtaining the exact composition of the PCT24 films (quantitative analysis). Despite this, the compositional profile of the films can be inferred once a steady-state situation is reached in the sample (Fig. 2). The presence of a lead gradient with a concentration increasing towards the substrate, accompanied by small fluctuations on this element content along the bulk film (and not on the other elements), can be deduced from the XPS measurements of this study (insets of Fig. 2). These results are in agreement with those shown by the RBS analyses, where besides the lead gradient detected (Figs. 4 and 5), a clear compositional discontinuity from one layer to another is observed when measurements with high resolution (7 MeV $^{14}N^+$ beam) are carried out on the films (Fig. 5). It must be pointed that this discontinuity is exclusively ascribed to the lead signal, as it was deduced from the compositional simulations carried out in the films. On the other hand, the binding energy spectra of the C 1s and O 1s core levels obtained by XPS reveal the presence of carbon-containing contaminants of different nature (e.g. graphitic carbon, hydrocarbons, carbonates) on the sample surface just at the beginning of the analysis (Fig. 3). This phenomenon, confirmed by numerous literature data,[33,34] is attributed to the accumulation of organic contaminants coming from the atmospheric ambient on the sample surface, prior to the Ar^+ bombardment. After 1 min of sputtering cleaning, carbonaceous contaminants are removed from the sample and the films surface appear totally free from carbon residuals, neither detecting carbon groups in the bulk film. One of the major drawbacks of the low-temperature processing of ferroelectric thin films is that the crystalline oxide phase is usually obtained together with organic residuals and/or non-ferroelectric secondary phases that lower (and even cancel) the electrical response of the material. In the particular case of the $(Pb_{1-x}Ca_x)TiO_3$ system, calcium carbonate ($CaCO_3$) can be formed during the thermal decomposition of the gel films, as observed in the counterpart ceramic powders.[35] This would suppose an additional problem, since carbonates from alkali and alkaline earth elements normally decompose at high temperatures, well above the processing temperature used in this work (450 ºC). The results of the C 1s signal obtained during depth profiling of the PCT24 films indicate the total absence of carbonaceous compounds (organic residuals, carbonates)

within the bulk film. The absorption of UV-light that leads to the electronic excitation of the organic species present in the gel-film, has promoted their quick decomposition and easier elimination from the network, even at temperatures such low as 450 ºC. From the XPS analysis it can be therefore concluded that PCT24 films without any organic rest can be obtained by PhotoChemical Solution Deposition at temperatures at which these organic species (mainly calcium carbonate) would remain in the system under conventional CSD processing. This result is confirmed by the XRD patterns of the films (Fig. 1). Second crystalline phases (e.g. polymorphs of $CaCO_3$, pyrochlore) are not detected under x-ray diffraction. A single-phase perovskite structure is obtained for the low-temperature processed films of this work, whose preferred orientation seems to be influenced by the local atmosphere at which they were processed (air or oxygen).

The compositional calculations carried out by RBS also reveal the significant effects produced by the low-temperature processing in the PCT24 films here shown (Figs. 4 and 5). The average elemental concentration simulated for each film (0.84 Pb + 0.24 Ca + 1.00 Ti + 3.08 O) presents a 10 mol% of lead excess respect to the stoichiometric composition of the expected perovskite ($Pb_{0.76}Ca_{0.24}TiO_3$). It must be noticed that this calculated composition is the same that the nominal composition of the synthesised precursor solution, which contained a 10 mol% of lead excess (0.836 Pb + 0.240 Ca + 1.000 Ti + 3.076 O). In the sol-gel chemistry of lead based-on ferroelectric compositions, this lead excess is normally introduced in the solution in order to compensate the loss of this element produced during the thermal annealing of the films at high temperatures. Thus, earlier studies[28] by RBS on PCT24 films processed at 650 ºC revealed that stoichiometric films are obtained when the initial lead excess of the precursor solution is lost by evaporation during the thermal annealing (see data corresponding to the PCT24-air* film in Table 1). However, the low processing temperature here used seems to minimise the volatilisation of this compound and therefore, both crystalline PCT24 films retain the 10 mol% of lead excess incorporated to the respective precursor solution. The total distribution of lead through the bulk film is not completely homogeneous, and a gradient on the concentration of this element with values increasing towards the inner layers is obtained from both XPS experimental analysis and RBS simulated data of the films. From this study, it is not possible to know where the lead excess is placed within the bulk film (grain boundaries, defective perovskite crystals, interfaces). However, we have evidence that it should not be

incorporated into the PCT24 perovskite crystals here formed. As the Pb^{2+} content introduced in the $(Pb_{1-x}Ca_x)TiO_3$ system is larger, the ferroelectric-paraelectric transition is displaced towards higher temperatures[36] until it reaches that of pure $PbTiO_3$ (Tc = 490 ºC). The transition temperature measured in these low-temperature processed films is close to that obtained in stoichiometric $Pb_{0.76}Ca_{0.24}TiO_3$ films prepared by conventional CSD at higher temperatures.[37] Therefore, it is expected the lead excess must be placed either in the grain boundaries or in the film-substrate interface of the films of this work. From these results, the ultraviolet sol-gel photoannealing technique has proved to be a feasible method for the soft fabrication of advanced functional materials (ferroelectric ceramics) reducing hazards volatilisation towards the atmosphere besides energy consumption and thermal load of the process. Furthermore, the conclusions here drawn could be extrapolated not only to other ferroelectric compositions based on the lead titanate perovskite, e.g. $Pb(Zr,Ti)O_3$ (PZT), $Pb(Mg,Nb)O_3$ (PMN), but also to ferroelectric lead-free compositions containing elements with high vapour pressure, e.g. $(Bi,Na)TiO_3$ (BNT), $SrBi_2Ta_2O_9$ (SBT), as volatile bismuth. Regarding the different thicknesses obtained in the films by XPS and RBS (see Table 1), the assumption of a sputter rate of 4.5 nm/min (Ta_2O_5) in the XPS analysis could introduce a deviation in the thickness calculation by this technique. On the other hand, thicknesses obtained by SEM[18] for the PCT24-air and PCT24-ox films (~280 and ~300 nm, respectively) are quite similar to those calculated by RBS (~272 and ~290 nm, respectively), which suggests that the thicknesses of the films should be within these values.

As it was stated in the Introduction, the thermal treatments used for the crystallisation of ferroelectric thin films normally promote the reaction between the substrate and the ferroelectric layer, thus resulting in the formation of detrimental interfaces in the film heterostructure.[28,38] This affects the electrical response of the material and hence deteriorates the functionality of the device.[39] The films of this work have developed an interface of Pt_xPb composition and 4 % of total film thickness (~11 nm), as deduced from the RBS analysis (see Table 1). This thickness is much lower than that of the interface usually formed in sol-gel derived PCT24 films processed by RTP at higher temperatures, which is near 15 % of total film thickness (see data corresponding to the PCT24-air* film in Table 1).[28,39] Note that in these films, an interlayer containing Pb, Ca, Ti, O, Pt elements is formed between the PCT24 film and the Pt bottom

electrode. The higher processing temperature (650 ºC) at which these films are processed is responsible for the larger diffusion of the constituent elements of the perovskite, thus leading to the formation of thicker interfaces. The low temperature at which the PCT24 films are here obtained by ultraviolet sol-gel photoannealing decreases significantly the interdiffusion between the ferroelectric layer and the Pt bottom electrode and therefore very fine interfaces are obtained. This reduction in the formation of detrimental interfaces is expected to improve the electrical properties (permittivity, remanent polarisation) of the ferroelectric thin films due to the approximation of an in-series capacitor (ferroelectric bulk film and non-ferroelectric interface), analogous to the "dead layer effect".[40] On the other hand, some authors have previously reported the non-planar nature of these Pb-Pt intermetallic layers.[22] The rough surface of this interlayer could be transmitted to the rest of the deposited layers. This would explain the irregular topography of the sample observed in the SEM micrograph in the inset of Fig. 4, which shows regions with different contrast ascribed to the presence of roughness at the surface of the film.[18]

Finally, despite the low-temperature processing (450 ºC) of the films of this work, they show appreciable dielectric and ferroelectric response. Higher processing temperatures would probably lead to films with improved electrical features (mainly due to the formation of larger grains), but theoretically incompatible with the temperatures demanded by the silicon technology. The dielectric and ferroelectric properties of the films here shown are however still high enough to fulfil the requirements for their use in electronic devices.[16] Furthermore, it has recently been shown that ozonolysis of the PCT24-ox films (produced by UV-irradiation in oxygen atmosphere) leads to an improvement on their electrical response.[18] As it can be observed in Table 1, higher values of the dielectric anomaly ($\Delta k'/\Delta T$) and lower coercive fields (E_c) are measured for the PCT24-ox film. The local atmosphere at which the films were processed (air or oxygen) certainly influences the electrical properties of the material. Oxygen (O_2) is readily dissociated under UV-light, forming ozone (O_3) and active oxygen species $O(^1D)$. Ozone is a strong oxidant agent that produces the rapid combustion of the organic compounds and the active oxygen species can react with suboxides, improving stoichiometry and decreasing the density of defects and oxygen vacancies. However, none effect of the processing atmosphere on the heterostructural features of the PCT24 films is deduced from the experimental XPS and

RBS analyses here carried out. Possible differences in the oxygen concentration of the films (due to the density of oxygen vacancies) are not easily detected by the aforementioned techniques. The uncertainty in XPS measurements for the elements concentration (10 %) as well as the poor detection of elements with small atomic number (e.g. oxygen) by RBS prevents the securing of such task. Further investigations are being carried out in our laboratory to study the influence of this lead excess (also its total absence) in the electrical properties of the PCT24-ox films fabricated at low temperatures by PhotoChemical Solution Deposition.

Conclusions

Full-crystalline perovskite $(Pb_{0.76}Ca_{0.24})TiO_3$ (PCT24) thin films have been obtained by ultraviolet sol-gel photoannealing (PhotoChemical Solution Deposition) at 450 ºC, using air and oxygen atmospheres. Analysis by XPS and RBS complementary techniques reveals consistent results about the particular heterostructure and compositional depth profile of these low-temperature processed films. Thus, the PCT24 films show a compositional in-depth profile with none organic rests still not decomposed within the bulk material. The low temperature used avoids the lead loss by volatilisation and minimises the interdiffusion between the ferroelectric layer and the Pt bottom electrode, thus resulting the formation of very fine interfaces of a Pt_xPb composition. Comparison between XPS and RBS (both low and high resolution measurements) results also indicates that the films have a lead gradient with a concentration increasing from the top to the bottom, and that small fluctuations on this element content are present along the bulk film. Although improved electrical properties are obtained in the films processed in oxygen, no difference between the heterostructural features of both films are detected by the experimental analyses carried out in this work.

Acknowledgment. This work has been supported by Spanish project MAT2004-02014 and European Network of Excelence: Multifunctional & integrated piezoelectric devices (NoE-MIND CE FP6 515757-2)

REFERENCES

(1) Setter, N.; Damjanovic, D.; Eng, L.; Fox, G.; Gevorgian, S.; Hong, S.; Kingon, A.; Kohlstedt, H.; Park, N. Y.; Stephenson, G. B.; Stolitchnov, I.; Taganstev, A. K.; Taylor, D. V.; Yamada, T. *J. Appl. Phys.* **2006**, *100*, 051606.

(2) Scott, J. F.; Araujo, C. A. *Science*, **1989**, *246*, 1400.

(3) Auciello, O.; Scott, F.; Ramesh, R. *Phys. Today* **1998**, *51(7)*, 22.

(4) *Semiconductor Industry Association. International Technology Roadmap for Semiconductors, 2005, International SEMATECH, Austín TX*; available at http://public.itrs.net.

(5) Ramesh, R.; Aggarwal, S.; Auciello, O. *Mat. Sci. Eng. R.* **2001**, *32(6)*, 191.

(6) Dawber, M.; Rabe, K. M.; Scott, J. F. *Rev. Mod. Phys.* **2005**, *77(4)*, 1083.

(7) Poyato, R.; Calzada, M. L.; Pardo, L. *Appl. Phys.* **2003**, *93(7)*, 4081.

(8) Kholkin, A. L.; Calzada, M. L. *J. Phys. IV* **1998**, *8*, 195.

(9) Kwoka, C. K.; Desu, S. B. *J. Mater. Res.* **1993**, *8(2)*, 339.

(10) Kato, K. *Jpn. J. Appl. Phys.* **1998**, *37*, 5178.

(11) Huang, Z.; Zang, Q.; Whatmore, R. W. *J. Mater. Sci. Lett.* **1998**, *17*, 1157.

(12) Celinska, J.; Joshi, V.; Narayan, S.; McMillan, L. D.; Paz de Araujo, C. A. *Integr. Ferroelectr.* **2000**, *30*, 1.

(13) Kosec, M.; Malic, B.; Mandeljc, M. *Mat. Sci. Semicon. Proc.* **2002**, *5(2-3)*, 97.

(14) Calzada, M. L.; González, A.; Poyato, R.; Pardo, L. *J. Mater. Chem.* **2003**, *13*, 1451.

(15) Wu, A.; Vilarinho, P. M.; Reaney, I.; Salvado, I. M. M. *Chem. Mater.* **2003**, *15(5)*, 1147.

(16) Calzada, M. L.; Bretos, I.; Jiménez, R.; Guillon, H.; Pardo, L. *Adv. Mater.* **2004**, *16(18)*, 1620.

(17) Imai, H. Ultraviolet (UV) Irradiation. In *Handbook of Sol-gel Science and Technology. Processing, Characterization and Applications*; Sakka, S., Ed.; Kluwer Academic Publishers: Boston, 2005; Vol. 1, Chapter 27, p 639.

(18) Calzada, M. L.; Bretos, I.; Jiménez, R.; Guillén, H.; Ricote, J.; Pardo, L. *J. Mater. Res.* **2007**, *22(7)*, 1824.

(19) Boyd, I. W.; Zhang, J. Y. *Solid. State Electron.* **2001**, *45*, 1413.

(20) Chen, S. Y.; Chen, I. W. *J. Am. Ceram. Soc.* **1994**, *77(9)*, 2332.

(21) Chen, S. Y.; Chen, I. W. *J. Am. Ceram. Soc.* **1998**, *81*, 97.

(22) Impey, S. A.; Huang, Z.; Patel, A.; Beanland, R.; Shorrocks, N. M.; Watton, R.; Whatmore, R. W. *J. Appl. Phys.* **1998**, *83(4)*, 2202.

(23) Huang, Z.; Zang, Q.; Whatmore, R. W. *J. Appl. Phys.* **1999**, *85*, 7355.

(24) Wu, A.; Vilarinho, P. M.; Salvado, I. M. M.; Baptista, J. L.; Zhou, Z.; Reaney, I.; Ramos, A. R.; da Silva, M. F. *J. Am. Ceram. Soc.* **2002**, *85(3)*, 641.

(25) Zhang, J. Y.; Boyd, I. W. *Jpn. J. Appl. Phys.* **1999**, *38*, L393.

(26) Zhang, X. D.; Meng, X. J.; Sun, J. L.; Lin, T.; Chu, J. H. *Appl. Phys. Lett.* **2005**, *86*, 252902.

(27) Mayer, M. *SIMNRA user's guide. Tech. Rep. IPP 9/113*, Max-Planck-Institut für Plasmaphysik, Garching, 1997.

(28) Sirera, R.; Leinen, D.; Rodriguez-Castellón, E.; Calzada, M. L. *Chem. Mater.* **1999**, *11(12)*, 3437.

(29) Bretos, I. *PhD Thesis* 2006, Universidad Autónoma de Madrid.

(30) Leinen, D.; Fernández, A.; Espinós, J. P.; González-Elipe, A. R. *Surf. Interface Anal.* **1993**, *20*, 941.

(31) Gopinath, C. S.; Hegde, S. G.; Ramaswamy, A. V.; Mahapatra, S. *Mater. Res. Bull.* **2002**, *37*, 1323.

(32) Kim, K. S.; O`Learly, T. J.; Winograd, N. *Anal. Chem.* **1973**, *45*, 2214.

(33) Blachard Jr., D. L.; Baer, D. R. *Surf. Sci.* **1992**, *276*, 27.

(34) Bukhtiyarov, V. I.; Nizovskii, A. I.; Bluhm, H.; Hävecker, M.; Kleimenov, E.; Knop-Gericke, A.; Schlögl, R. *J. Catal.* **2006**, *238*, 260.

(35) Calzada, M. L.; Malic, B.; Sirera, R.; Kosec, M. *J. Sol-Gel Sci. Techn.* **2002**, *23*, 221.

(36) Mendiola, J.; Jiménez, B.; Alemany, C.; Pardo, L.; Del Olmo, L. *Ferroelectrics* **1989**, *94*, 183.

(37) Mendiola, J.; Calzada, M. L.; Ramos, P.; Martín, M. J.; Agulló-Rueda, F. *Thin Solid Films* **1998**, *315*, 195.

(38) Calzada, M. L.; Jiménez, R.; González, A.; García-López, J.; Leinen, D.; Rodríguez-Castellón, E. *Chem. Mater.* **2005**, *17*, 1441.

(39) Calzada, M. L.; Bretos, I.; Jiménez, R.; Ricote, J.; Mendiola, J.; García-López, J.; Respaldiza, M. A. *J. Am. Ceram. Soc.* **2005**, *88(12)*, 3388.

(40) Zhou, C.; Newns, D. M. *J. Appl. Phys.* **1997**, *82(6)*, 3081.

Table 1. Summary of X-ray Photoelectron Spectroscopy (XPS) and Rutherford Backscattering Spectroscopy (RBS) data together with electrical properties obtained in the PCT24 films processed by PhotoChemical Solution Deposition (PCSD) at 450 ºC and conventional Chemical Solution Deposition (CSD) at 650 ºC

		Oxide film		Bottom interface		Film thickness		Electrical properties [18]		
Nominal composition of the precursor solution	Film	Average elemental composition from RBS (1)	Percentage of film thickness from RBS	Composition from RBS (1)	Percentage of film thickness from RBS	XPS (nm)	RBS (2) (nm)	$\Delta k'/\Delta T$ x 10^3 (3)	P_r ($\mu C/cm^2$)	E_c (kV/cm)
$(Pb_{0.76}Ca_{0.24})TiO_3$ + 10 mol% PbO [0.836 Pb + 0.240 Ca + 1.000 Ti + 3.076 O]	PCSD processed films at 450 ºC									
	PCT24-air	0.84 Pb + 0.24 Ca + 1.00 Ti + 3.08 O*	96%	Pt_xPb	4%	~195	~272	~570	~11	~225
	PCT24-ox	0.84 Pb + 0.24 Ca + 1.00 Ti + 3.08 O*	96%	Pt_xPb	4%	~205	~290	~1059	~11	~165
	CSD processed films at 650 ºC [28,29]									
	PCT24-air*	0.77 Pb + 0.24 Ca + 1.00 Ti + 3.01 O*	87%	Pb-Ca-Ti-O-Pt	13%	-	~400	-	~25	~75

(1) Error of ~10 %. The formation of films with perovskite structure is assumed

(2) Thickness was calculated considering the theoretical density of the $(Pb_{0.76}Ca_{0.24})TiO_3$ perovskite

(3) Normalised dielectric anomaly ($\Delta k'$; difference between the dielectric constant measured at Tm (temperature of k' maximum) and that corresponding at room temperature)

* The atomic concentration of oxygen has been determined from the atomic concentrations calculated by RBS in the metal cations (Pb, Ca, Ti)

Captions for Figures

Figure 1. X-Ray Diffraction (XRD) patterns of the low-temperature processed PCT24 films (Pv: perovskite, Pt: platinum, *: substrate)

Figure 2. Atomic concentrations of constituent elements obtained by X-ray Photoelectron Spectroscopy (XPS) during depth profiling of the low-temperature processed PCT24-air (a) and PCT24-ox (b) films. Insets show the individual Pb 4f signal obtained during depth profiling of the respective films

Figure 3. Photoelectron C 1s (a) and O 1s (b) core levels measured in the low-temperature processed PCT24-air film as a function of depth and binding energy

Figure 4. Low-energy (3 MeV $^{4}He^{2+}$) Rutherford Backscattering Spectroscopy (RBS) spectra of the low-temperature processed PCT24-air film. Inset shows plan-view micrograph of the film obtained by Scanning Electron Microscopy (SEM)

Figure 5. High-energy (7 MeV $^{14}N^{+}$) Rutherford Backscattering Spectroscopy (RBS) spectra and corresponding heterostructure of the low-temperature processed PCT24-air (a) and PCT24-ox (b) films

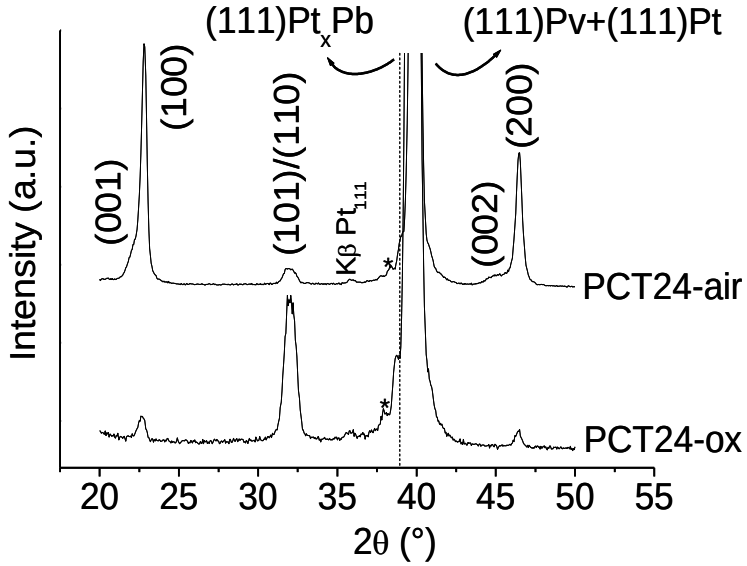
(111)Pt$_x$Pb
(111)Pv+(111)Pt
(001)
(100)
(101)/(110)
Kβ Pt$_{111}$
(002)
(200)
*
*
PCT24-air
PCT24-ox
Intensity (a.u.)
20
25
30
35
40
45
50
55
2θ (°)

Figure 1

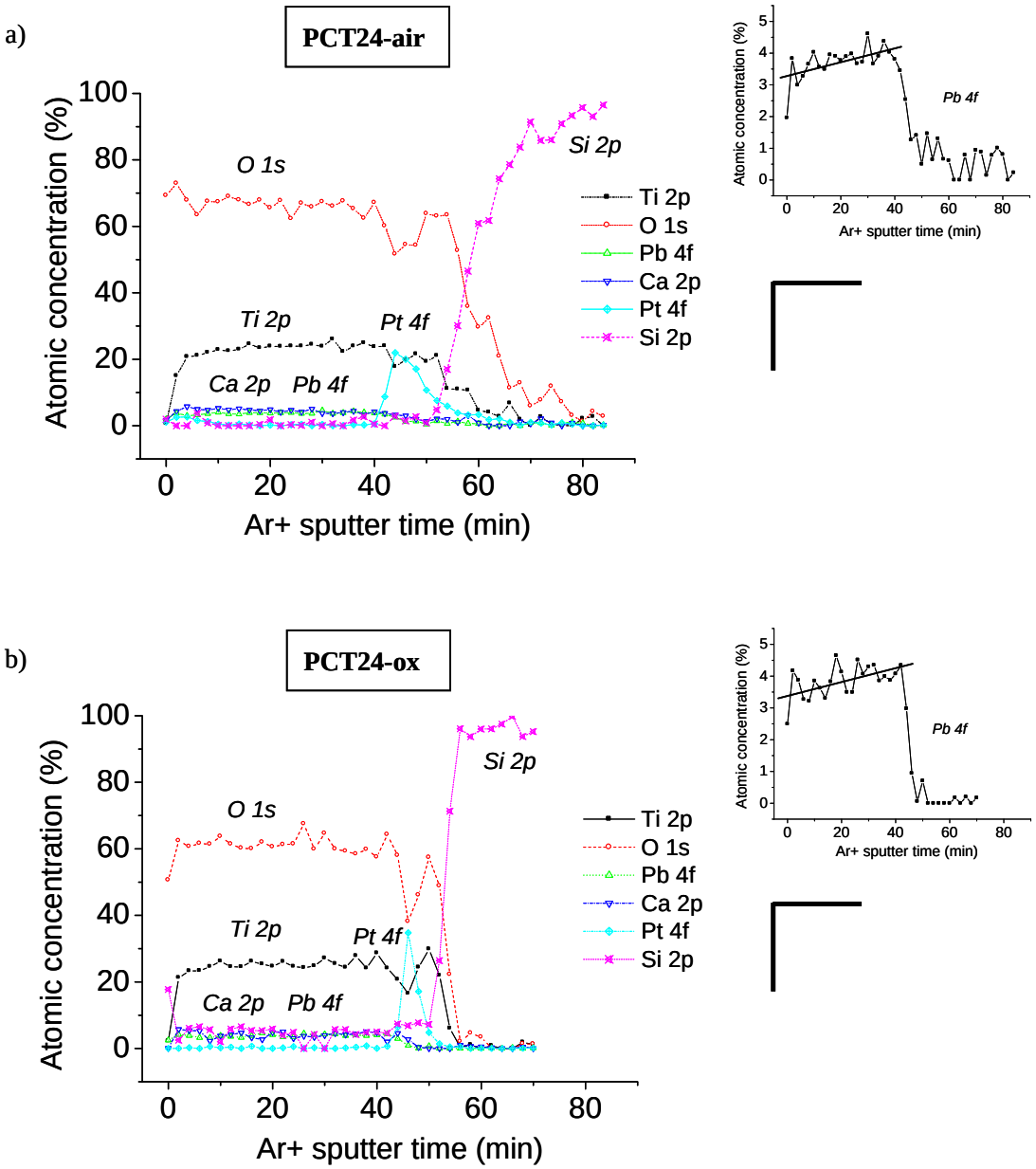
a)
PCT24-air
Atomic concentration (%)
Ar+ sputter time (min)
O 1s
Si 2p
Ti 2p
Pt 4f
Ca 2p
Pb 4f
Ti 2p
O 1s
Pb 4f
Ca 2p
Pt 4f
Si 2p
Pb 4f
b)
PCT24-ox
Atomic concentration (%)
Ar+ sputter time (min)
O 1s
Si 2p
Ti 2p
Pt 4f
Ca 2p
Pb 4f
Ti 2p
O 1s
Pb 4f
Ca 2p
Pt 4f
Si 2p
Pb 4f

Figure 2

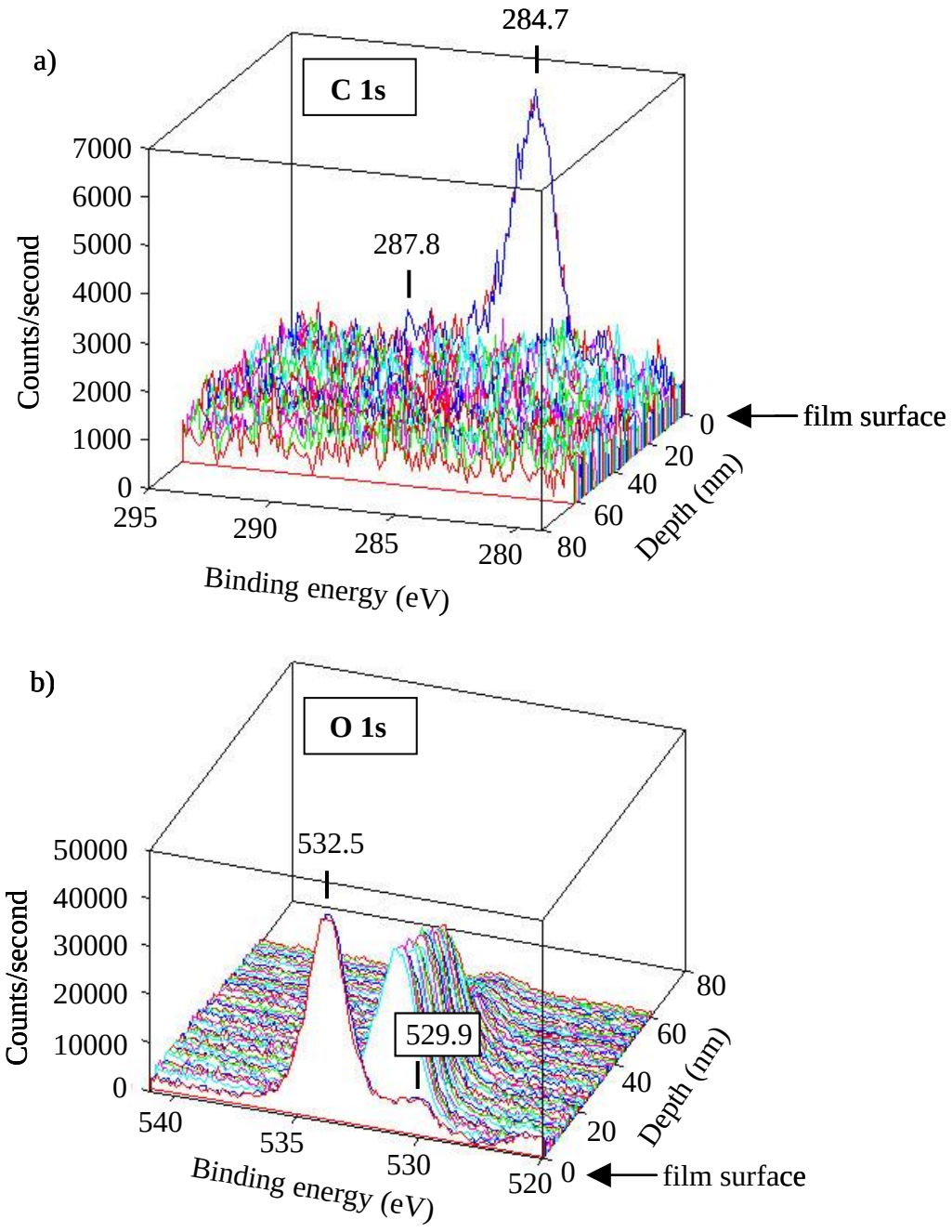
a)
C 1s
284.7
287.8
Counts/second
7000
6000
5000
4000
3000
2000
1000
0
295
290
285
280
Binding energy (eV)
80
60
40
20
0
Depth (nm)
film surface
b)
O 1s
532.5
529.9
Counts/second
50000
40000
30000
20000
10000
0
540
535
530
520
Binding energy (eV)
80
60
40
20
0
Depth (nm)
film surface

Figure 3

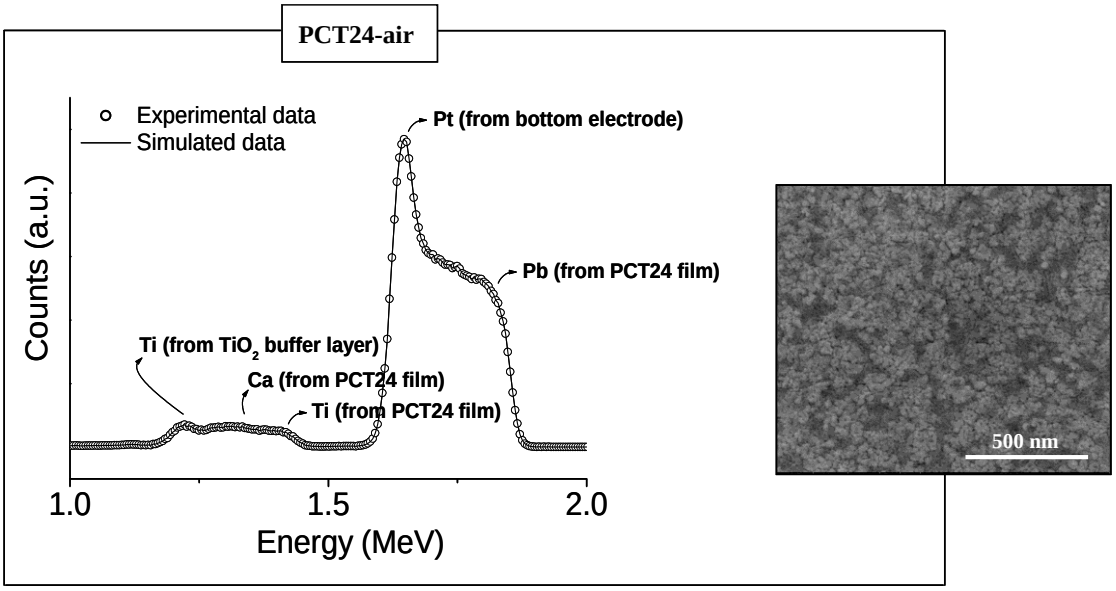
PCT24-air
Experimental data
Simulated data
Pt (from bottom electrode)
Pb (from PCT24 film)
Ti (from TiO2 buffer layer)
Ca (from PCT24 film)
Ti (from PCT24 film)
Counts (a.u.)
1.0
1.5
2.0
Energy (MeV)
500 nm

Figure 4

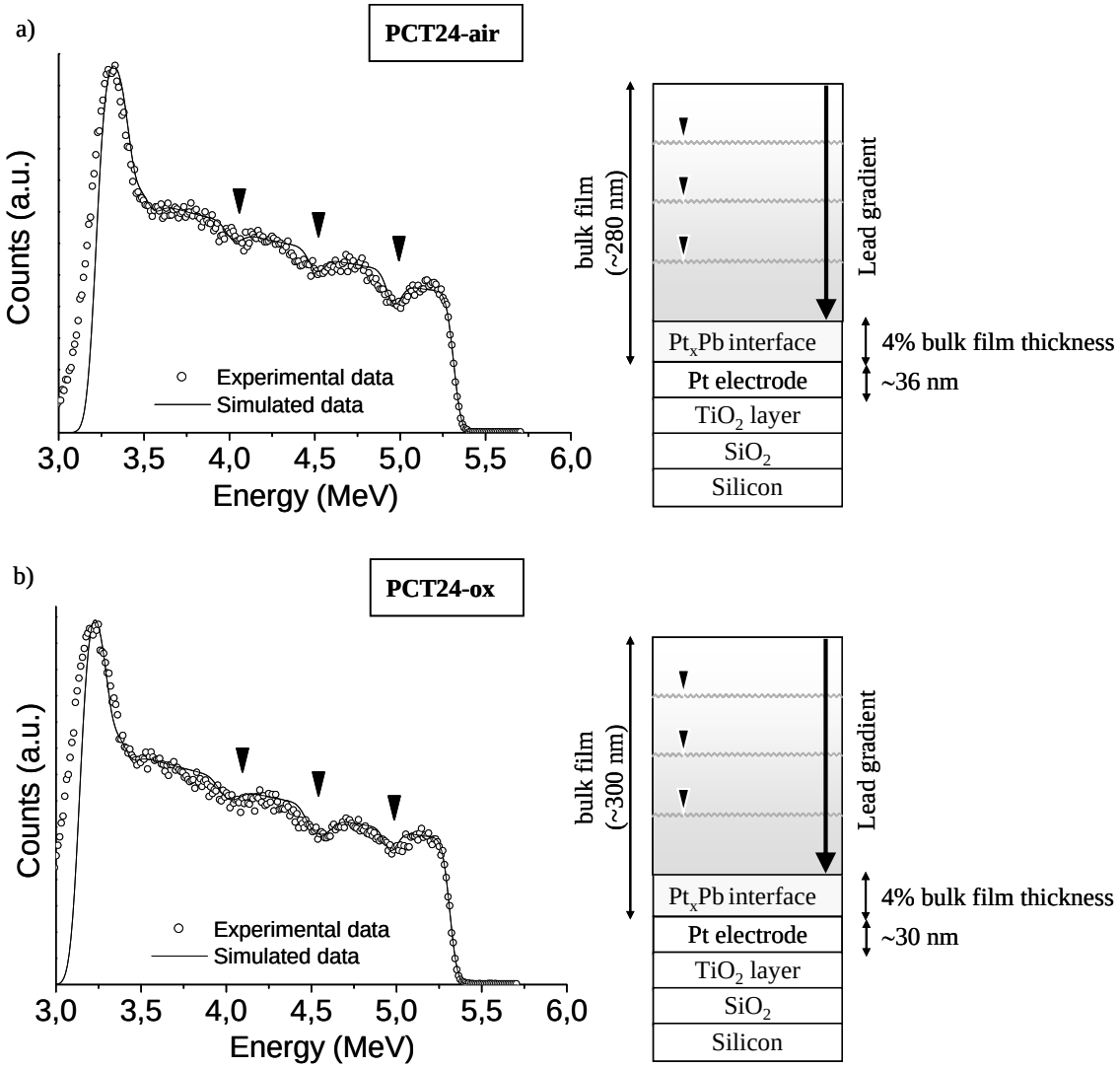
a)
PCT24-air
Counts (a.u.)
Experimental data
Simulated data
3,0
3,5
4,0
4,5
5,0
5,5
6,0
Energy (MeV)
bulk film
(~280 nm)
Lead gradient
Pt$_x$Pb interface
Pt electrode
TiO$_2$ layer
SiO$_2$
Silicon
4% bulk film thickness
~36 nm
b)
PCT24-ox
Counts (a.u.)
Experimental data
Simulated data
3,0
3,5
4,0
4,5
5,0
5,5
6,0
Energy (MeV)
bulk film
(~300 nm)
Lead gradient
Pt$_x$Pb interface
Pt electrode
TiO$_2$ layer
SiO$_2$
Silicon
4% bulk film thickness
~30 nm

Figure 5